Short communication

Investigating the adsorption, electronic properties, and gas-sensing responses of NH₃ on the B₃S monolayer

Mohamed J. Saadh [a], Sura Mohammad Mohealdeen [b], Nelly Esther Flores Tapia [c], Shelesh Krishna Saraswat [d,*], Byron Stalin Rojas Oviedo [e], Linda Mariuxi Flores Fiallos [f], Miguel Escobar [g], Yasser Elmasry [h]

[a] Faculty of Pharmacy, Middle East University, Amman 11831, Jordan
[b] Department of Radiology & Sonar Techniques, Al-Noor University College, Nineveh, Iraq
[c] Research and Development Directorate, Faculty of Sciences, Food and Biotechnology, Technical University of Ambato, Ambato, Ecuador
[d] Department of Electronics and Communication GLA University, Mathura 281406, India
[e] Escuela Superior Politécnica de Chimborazo (ESPOCH), Grupo de Investigación GITAFEC, Riobamba 060155, Ecuador
[f] Escuela Superior Politécnica de Chimborazo (ESPOCH), Grupo de Investigación GIADE, Riobamba 060155, Ecuador
[g] Mechanical Engineering, Escuela Superior Politécnica de Chimborazo (ESPOCH), Riobamba 060155, Ecuador
[h] Department of Mathematics, Faculty of Science, King Khalid University, P.O. Box 9004, Abha 61466, Saudi Arabia

ARTICLE INFO

ABSTRACT

Finding a suitable sensing material for NH₃ has been considered to be scientifically important. In order to thoroughly understand the possibility of using a B₃S monolayer (B₃SML) as a sensor for detecting NH₃, the adsorption behaviors, optical, gas sensing and electronic attributes of NH₃ and other gas molecules were inspected on the B₃SML by performing DFT calculations. Based on the results, the gas sensing performance of the pristine B₃SML in detecting NH₃ was good. Also, the results on the adsorption behaviors (adsorption modes, geometric structures and adsorption energies), optical/electronic attributes, electron density differences and charge transfer indicated the potential application of the B₃SML as a NH₃ sensor. Overall, the B₃SML can be regarded as an ideal sensing material to detect NH₃. The current work can provide insights into the interactions between gases and surfaces, which can be conducive to developing two-dimensional materials for detecting NH₃.

1. Introduction

One of the detrimental threats to the humans and the environment is the release of toxic gasses from different sources such as chemical and combustions reactions as well as industrial factories. One of these gasses and compounds which is used in manufacturing chemicals and industrial cleansing is ammonia (NH₃) [1–4]. Furthermore, NH₃ has widespread application in diagnosing various diseases such as lung cancer, malignant tumors, kidney diseases and diabetes. In spite of its benefits, the toxicity of NH₃ is high, which can be detrimental to the human life. For instance, people who are exposed to 25 ppm of this gas suffer from lung, eye and skin irritations [5]. Also, a high concentration of NH₃ can be poisonous [6]. So, monitoring and detecting NH₃ and its concentration are considered significant, which necessitates the urgent development and design of promising materials for its detection.

In recent years, following the successful exfoliation of graphene (Gr)

thanks its unique attributes, including high chemical stability, low electronic temperature noise and high mobility [7–22], two-dimensional (2D) nanomaterials have been employed as ideal sensors for the detection of various gasses [7–19,23–26]. Nevertheless, pure Gr lacks a bandgap, which limits its application as a suitable gas sensor. One of the most promising types of materials for chemical sensors are two-dimensional (2D) ones. Their unique properties, such as high surface to volume ratio, tunable conductivity, high sensitivity, selectivity, reversibility, and stability, make them ideal candidates for gas sensing applications. Graphene, in particular, is a promising gas sensing material due to its high surface area and high conductivity [27]. It has recently been used for detecting a variety of gases, such as NO₂, H₂, CO, SO₂, and S [28–33]. Other 2D materials, such as BN [34], C₃N [35], and carbon nanostructures [36–39], have also been studied for NH₃ detection, with mixed results. The studies show that NH₃ interacts weakly with the monolayers of these materials. One of the effective ways of improving

the gas sensing attributes of 2D materials is substitutional doping [8–10]. As an instance, B_2S [40], C_2N [41–43], siligraphene [44–46], and [1,1] paracyclophane [47] are common 2D materials ideal for hydrogen storage materials. Nevertheless, the gravimetric density and hydrogen adhesion energies of most pure 2D materials are low, limiting their application as a hydrogen storage material [48–52]. To solve this problem, researchers have functionalized them using metals such as Ti, Sc, Ca and Li [40,44,53–58]. Here, the metal atoms are adhered chemically onto these materials for increasing the adhesion strength of hydrogen molecule. Li-decorated B_2S [40], C_2N [42] and triphenylene-graphdiyne [59], Ti-decorated Gr [55], B_2C [60], and 4-*tert*-butylcalix [61] arene [62], and Mg-decorated C_2N monolayer [63] are among ideal hydrogen storage materials. Researchers have recently used the particle swarm optimization (PSO) algorithm in order to design a Gr-like B_3S monolayer (B_3SML). They demonstrated that B_3SML is thermally, mechanically and dynamically stable with a higher cohesive energy in comparison with other isomers [64]. The fascinating structure of the B_3S monolayer is stabilized by a sulfur atom to form a honeycomb structure, resembling graphene, silicene, germanene, and stanene. One notable difference is that boron has one fewer electron than group 14 elements [64].

Within the current study, the optoelectronic attributes and the adhesion behaviors of gas molecules were investigated over the most stable B_3SML to investigate its potential application as a sensor for detecting NH_3 by performing DFT calculations. Based on the results, the NH_3 sensing performance of the pristine B_3SML was good.

2. Computational details

Using the basis set 6-31G (d) and the functional B3LYP within GAMESS program, energy optimizations, full geometry, of the pristine B_3SML were performed [65]. To increase the accuracy of computations, particularly noncovalent interactions, we added the empirical dispersion term, B3LYP-D3. The above-mentioned basis set has been commonly used in the experimental synthesis of nanostructures [66,67]. Moreover, it can provide reliable and accurate calculational results regarding III–V semiconductors [68]. The convergence criterion for the self-consistent field (SCF) has been set to 10^{-6} for the optimizations. In addition, to ensure reliable results, structural changes were limited, with a maximum displacement of one coordinate set to 1.8×10^{-4} and an average (RMS) change of 1.2×10^{-4} overall structural parameters. The maximum remaining force on an atom and the average root mean square (RMS) force on all atoms have also been set to 4.5×10^{-4} and $3.0 \times$

10^{-4}, respectively. The DOS analysis was performed using the GaussSum program [69]. We also computed the electron density difference (EDD) and the Hirshfeld method was adopted to compute the charge transfer between the B_3SML and the gas molecules.

Moreover, the adhesion energy was computed as follows:

$$E_{ads} = E_{total} - E_{B3S} - E_{gas} \tag{1}$$

Here, E_{total} is total energy of the gas molecule adhered onto the pristine B_3SML E_{B3S} represents the energy of the pristine B_3SML and E_{gas} represents the energy of the adhered molecules. Here, a negative value demonstrated the exothermic nature of the adhesion.

3. Results and discussions

3.1. The adhesion of molecules onto the pristine B_3SML

As shown in Fig. 1a, the B_3SML was optimized. Having a lattice constant of a = 5.27 Å and b = 6.08 Å, the B_3SML contains an orthogonal primitive cell. B-B and B-S bonds, respectively, had a length of 1.663–1.681 Å and 1.820–1.849 Å, whereas the bond angles of B-B-B, B-B-S and B-S-B, respectively, were 126.1°, 113.9° and 120°. Based on its structural properties, the B_3SMML is anisotropic. The electronic properties of the B_3SML are shown in in Fig. 1b. The B_3SML possesses metallic attributes since its valence band passes via the Fermi level (FL). The findings obtained on the B_3SML are similar to those obtained in the literature [64].

Next, the adhesion of NH_3 onto the pristine B_3SML was investigated to examine the gas sensing attributes of the pristine B_3SML. Fig. 2 shows the most stable configuration of NH_3 adhered onto the B_3SML. The NH_3 molecule had a chemical adsorption onto the B_3SML in both B and S site and the adhesion energy were −0.247 and −1.079 eV for S and B sites (Table 1), respectively. Moreover, the chemical adsorption of NH_3 dramatically changed the electronic attributed of the B_3SML, thus leading to a significant amount of charge transport (0.204 e) between B_3SML and NH_3. Based on the results, the pristine B_3SML can be considered a promising sensor to detect NH_3. In comparison with other two-dimensional nanosheets used as ammonia sensors, the B_3S nanosheet demonstrates higher absorption energy. Additionally, the changes in the bandgap after ammonia absorption are also greater in the present work compared to other two-dimensional compounds (see Table 3).

Furthermore, the adhesion of other molecules such as H_2O, CO_2 and CH_4 were investigated on the B_3SML, and the results were given in Table 2. All of these molecules had a physical adhesion on the
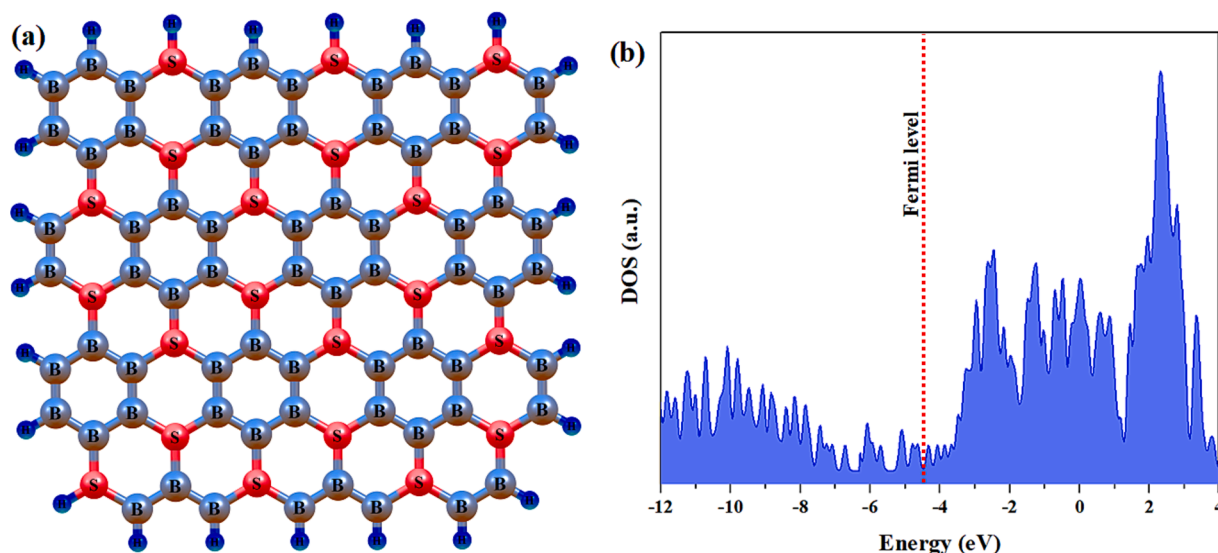
Fig. 1. (a) The optimized structure of B_3SML, (b) density of states (DOS), respectively. The reed dotted line shows the Fermi level.
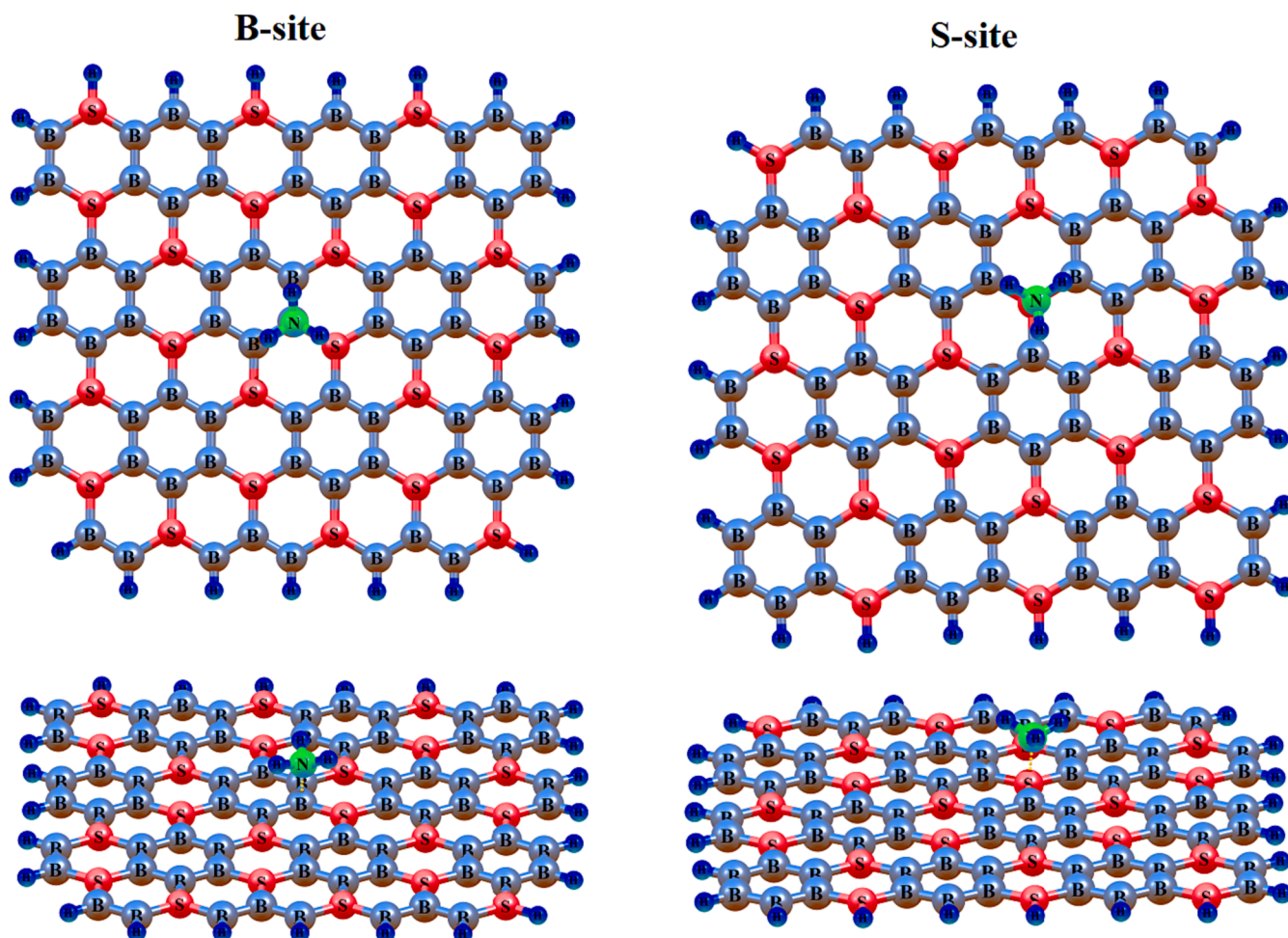
Fig. 2. Top and side views of the most stable configurations for the pristine B_3SML adsorption with NH_3 molecule.

Table 1
Adhesion energies (E_{ads}), charge transport from the B_3SML to every molecule (ΔQ), bandgap widths (E_g), and workfunction (Φ) for the structures of NH_3 adhered onto B_3SML.

Parameter	B_3S	B_3S-NH_3 (S site)	B_3S-NH_3 (B site)
E_{ads} (eV)	–	−0.427	−1.079
ΔQ (e)	–	−0.109	0.204
E_g (eV)	METAL	0.302	0.547
Φ (eV)	4.298	4.012	3.706

Table 2
Adhesion energies (E_{ads}), charge transport from the B_3SML to every molecule (ΔQ), bandgap widths (E_g), and workfunction (Φ) for the structures of molecules adhered onto B_3SML.

Molecules	E_{ads} (eV)	ΔQ (e)	E_g (eV)	Φ (eV)
CH_4	−0.193	0.041	METAL	4.298
CO_2	−0.213	0.067	0.168	4.285
H_2O	−0.384	0.056	0.233	4.170

Table 3
Adhesion energies (E_{ads}), charge transport and E_g of version 2D material sensor for NH_3.

System	E_{ads} (eV)	Q (e)	E_g (eV)	Ref
B_3S	−1.079	−0.109	0.547	This work
Siligene	−0.67	–	–	[74]
Germanene	−0.39	–	–	[75]
Stanane	−2.48	−0.017	0.75	[76]
$MoTe_2$	−0.24	−0.03	1.10	[77]

3.2. Analysis of electronic attributes

Here, the electronic attributes such as DOSs and band structures of the most stable CFG of NH_3 on the B_3SML were explore to understand the interactions between NH_3 and the B_3SML (see Fig. 3). In comparison to the electronic attributes of the pristine B_3SML, the adhesion of NH_3 altered the electronic attributes of the B_3SML. As shown in Fig. 3, for the structure of NH_3-BS_3 3, NH_3 not only introduced fully occupied states at ~ -6.7 eV under the FL in the valence bands, but also resulted in some impurity states at ~ 2.5 eV above the FL in the conduction bands (CBs), resulting in robust interactions between NH_3e and B_3SML, In line with the adhesion energies. Furthermore, the adhesion of NH_3 changed the bandgap of NH_3-B_3S to 0.547 eV. This was larger compared to the bandgap of the pristine B_3SML, which indicated that the bandgap was enlarged after the adhesion of NH_3. Similar properties have been found for the adhesion of molecules and atoms onto group-IV monolayers [70]. The valence band is the highest energy band in a solid material

monolayer since the adhesion energy was small, the charge transport was negligible, and there was no structural deformation. More importantly, the physical adhesion of these molecules did not significantly change the optoelectronic and magnetic attributes of the B_3SML, apart from H_2O. As shown in Table 2, the workfunction of the B_3SML changed to 4.170 eV following the physical adhesion of H_2O, which indicated that the physical adhesion of H_2O changed the attributes of B_3SML.

Fig. 3. The density of states (DOS) for NH_3 adsorbed on B_3SML.

containing valence electrons, while the Fermi level is the energy level at which there is a 50 % chance of finding an electron. The metallic properties of solid materials are closely related to the activity of valence electrons and the Fermi level. In metals, the valence bands overlap with the conduction bands, creating a continuous range of energy levels available for electrons to move through the material. This results in excellent electrical conductivity and excellent mobility. The Fermi level in metals lies in the overlap of the valence conduction bands and is closely related to the density of states at the Fermi level. High density of states at the Fermi level leads to high electrical conductivity and metallic properties. Additionally, changes in metal properties, such as conductivity or resistance, can be attributed to changes in the Fermi level due to external factors such as temperature or doping. Therefore, the Fermi level plays an important role in understanding the behavior of metallic materials. The adhesion of NH_3 induced some impurity states in the CBs by the FL and, most significantly, there was a shift in the FL into the initial CBs, which led to a change from conducting into semiconducting behaviors because of the adhesion of NH_3, which is one of the suitable properties for the application in sensors.

As shown in Fig. 4, the EDDs were computed and plotted for the most stable CFGs of NH_3 adhered onto the B_3SML. Useful information can be obtained based on the EDDs regarding the change transport between the B_3SML and NH_3. Electrons were transferred from the NH_3 to the B_3SML after the adhesion of NH_3 onto the B_3SML. The results obtained agree well with those of the Hirshfeld charge analysis. In comparison to the EDD of B_3SMLwithout the adhesion of NH_3, there was a reshuffling of electron densities surrounding the interaction regions between NH_3 and the B_3SML, which indicated that there was a robust interaction between NH_3 and B_3SML.

We can define the workfunction (Φ) as follows:

$$\Phi = E_{vac} - E_F \tag{2}$$

Here, the FL energy and vacuum energy level are designated by E_{vac} and E_F, respectively. One of the parameters in evaluating the possibility

of using materials as gas sensors is the workfunction [19,31,36]. of the workfunction of the B_3SML was 4.298 eV. The workfunction computed for different molecules is provided in Tables 1 and 2. Following the chemical adhesion of NH_3, the workfunction of the B_3SML decreased 3.706 eV, which indicated the prevention of electron transport to the vacuum level. Nonetheless, the workfunction did not change after the physical adsorption of CH_4, CO_2, and H_2O onto the B_3SML and the physical adsorption of NH_3 onto B_3SML. Hence, the selective adhesion of NH_3 could change the workfunction of the B_3SML, thus making it a suitable gas sensor.

3.3. ELF analysis

Becke and Edgecombe developed the Electron Localization Function (ELF) concepts for atomic and molecular systems as a complement to Silvi and Savin's ELF attractors for chemical bonds. In this study, the ELF was examined using bond critical points (BCPs) localization in all active sites [71]. The ELF maps were generated using B3LYP-D3 and displayed in Fig. 5, calculated along the (YZ) plane. The results showed that electron localization was highest at the upper edge level, where the S atom was located. The graph revealed that critical points localized between the N and S atoms had the greatest electron localization in bonding regions. These findings support the presence of non-covalent interaction forces between B_3S and NH_3 gas.

3.4. Recovery time

Recovery time (RT) of sensing materials is another important criterion in evaluating the performance of a gas sensor. Based on the transition state theory, there is a relationship between the adhesion energy and recovery time (τ) as follows:

$$\tau = \nu_0^{-1} e^{-Eads/kT} \tag{3}$$

where T, k, and ν_0, respectively, are the temperature, Boltzmann
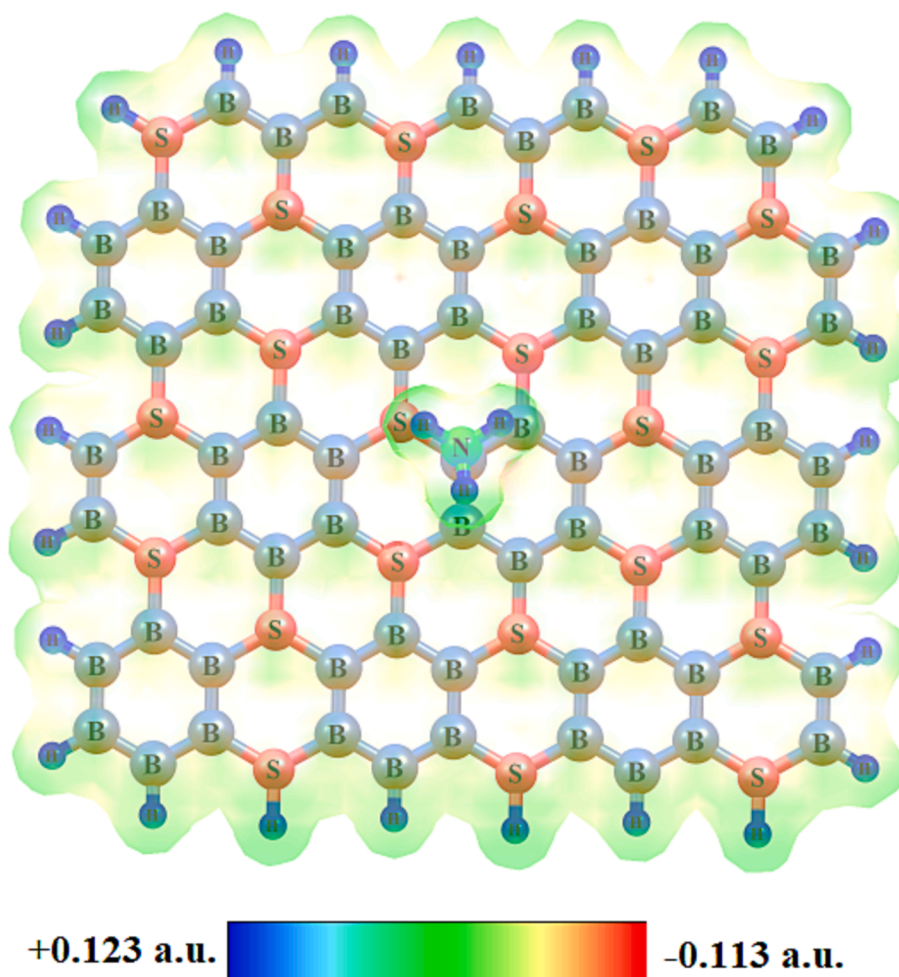
Fig. 4. The electron density difference for NH_3 adsorbed on B_3SML.
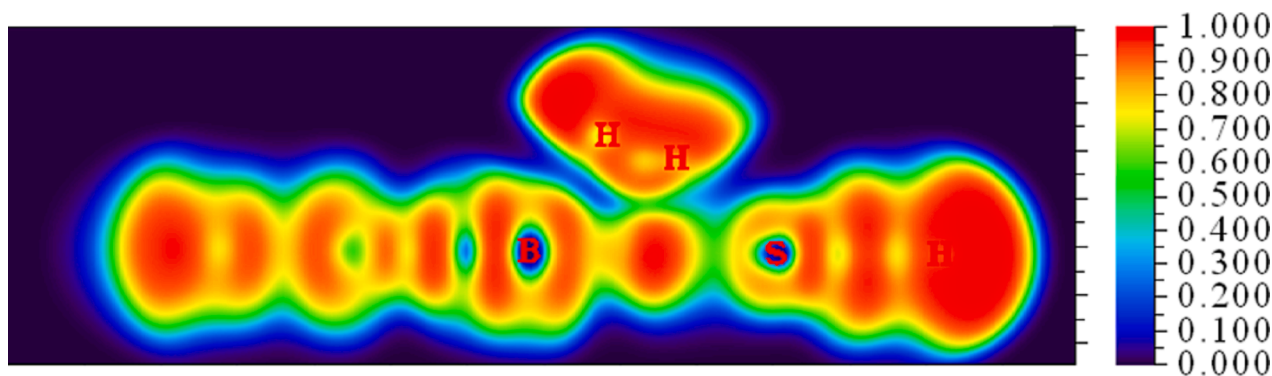
Fig. 5. The ELF map for NH_3 adsorbed on B_3SML.

constant and the attempted frequency. According to this equation, the higher the adhesion energy, the longer the RT [72]. The RT could be obtained at 300 K for $\nu_0 = 10^{12}$ s^{-1}. The RT of the B_3SML for NH_3 was 5.6×10^{15} s at 300 K. This was too long for preventing NH_3 to desorb from the B_3SML, i.e., a long RT can prevent the reusability of sensors to detect NH_3. According to Schedin et al., Gr-based sensors can be recovered to their initial geometries at 423 K through annealing within the RT of 100–200 s [73]. So, the RT was computed at 400 K. The RT of the B_3SML was between 0.389 s at 400 K. Based on the results, by raising the operating temperature we can overcome a long RT.

4. Conclusion

To thoroughly understand the potential of employing the B_3SML as a sensor for detecting NH_3, the adsorption behaviour, optical, gas sensing and electronic attributes of NH_3 and other gas molecules were checked over the B_3SML through DFT calculations. Based on the results, NH_3 had a chemical adhesion on the pristine B_3SML with a significant amount of adhesion energy and charge transport, which indicated that the gas sensing performance of B_3SML was good. The chemical adhesion significantly altered the optoelectronic attributes of the B_3SML. In addition, CH_4, CO_2 and H_2O had a physical adhesion onto the B_3SML and

negligibly changed the optoelectronic attributes of the B₃SML. The theoretically obtained results suggested that the B₃SML was a promising candidate for NH₃ sensors.

Declaration of Competing Interest

The authors declare that they have no known competing financial interests or personal relationships that could have appeared to influence the work reported in this paper.

Data availability

No data was used for the research described in the article.

Acknowledgments

References

[1] M. Shahabuddin, A. Sharma, J. Kumar, M. Tomar, A. Umar, V. Gupta, Metal clusters activated SnO2 thin film for low level detection of NH3 gas, Sens. Actuators B: Chem. 194 (2014) 410–418.

[2] C. Liu, Z. Duan, B. Zhang, Y. Zhao, Z. Yuan, Y. Zhang, Y. Wu, Y. Jiang, H. Tai, Local Gaussian process regression with small sample data for temperature and humidity compensation of polyaniline-cerium dioxide NH3 sensor, Sens. Actuators B: Chem. 378 (2023), 133113.

[3] X. Duan, Z. Duan, Y. Zhang, B. Liu, X. Li, Q. Zhao, Z. Yuan, Y. Jiang, H. Tai, Enhanced NH3 sensing performance of polyaniline via a facile morphology modification strategy, Sens. Actuators B: Chem. 369 (2022), 132302.

[4] F. Yu, S. Yu, C. Li, Z. Li, F. Song, Z. Xu, Y. Zhu, C. Dai, X. Cao, Z. Zhang, Molecular engineering of biomimetic donor-acceptor conjugated microporous polymers with full-spectrum response and an unusual electronic shuttle for enhanced uranium (VI) photoreduction, Chem. Eng. J. 466 (2023), 143285.

[5] O. Goertz, A. Popp, J. Kolbenschlag, J. Vogelpohl, A. Daigeler, A. Ring, M. Lehnhardt, T. Hirsch, Intravital pathophysiological comparison of acid-and alkali-burn injuries in a murine model, J. Surg. Res. 182 (2013) 347–352.

[6] J.-W. Yoon, J.-H. Lee, Toward breath analysis on a chip for disease diagnosis using semiconductor-based chemiresistors: Recent progress and future perspectives, Lab Chip 17 (2017) 3537–3557.

[7] L. Kou, T. Frauenheim, C. Chen, Phosphorene as a superior gas sensor: selective adsorption and distinct I-V response, J. Phys. Chem. Lett. 5 (2014) 2675–2681.

[8] S.S. Varghese, S. Lonkar, K. Singh, S. Swaminathan, A. Abdala, Recent advances in graphene based gas sensors, Sens. Actuat. B: Chem. 218 (2015) 160–183.

[9] C. Rao, K. Gopalakrishnan, U. Maitra, Comparative study of potential applications of graphene, MoS₂, and other two-dimensional materials in energy devices, sensors, and related areas, ACS Appl. Mater. Interfaces 7 (2015) 7809–7832.

[10] P.K. Kannan, D.J. Late, H. Morgan, C.S. Rout, Recent developments in 2D layered inorganic nanomaterials for sensing, Nanoscale 7 (2015) 13293–13312.

[11] C. Tan, X. Cao, X.-J. Wu, Q. He, J. Yang, X. Zhang, J. Chen, W. Zhao, S. Han, G.-H. Nam, Recent advances in ultrathin two-dimensional nanomaterials, Chem. Rev. 117 (2017) 6225–6331.

[12] L. Kou, C. Chen, S.C. Smith, Phosphorene: fabrication, properties, and applications, J. Phys. Chem. Lett. 6 (2015) 2794–2805.

[13] S. Yang, C. Jiang, S.-H. Wei, Gas sensing in 2D materials, Appl. Phys. Rev. 4 (2017).

[14] V. Babar, S. Sharma, U. Schwingenschlögl, New paradigm for gas sensing by two-dimensional materials, J. Phys. Chem. C 123 (2019) 13104–13109.

[15] S.S. Varghese, S.H. Varghese, S. Swaminathan, K.K. Singh, V. Mittal, Two-dimensional materials for sensing: graphene and beyond, Electronics 4 (2015) 651–687.

[16] C. Anichini, W. Czepa, D. Pakulski, A. Aliprandi, A. Ciesielski, P. Samorì, Chemical sensing with 2D materials, Chem. Soc. Rev. 47 (2018) 4860–4908.

[17] Z. Meng, R.M. Stolz, L. Mendecki, K.A. Mirica, Electrically-transduced chemical sensors based on two-dimensional nanomaterials, Chem. Rev. 119 (2019) 478–598.

[18] B. Liu, K. Zhou, Recent progress on graphene-analogous 2D nanomaterials: properties, modeling and applications, Prog. Mater. Sci. 100 (2019) 99–169.

[19] M. Donarelli, L. Ottaviano, 2D materials for gas sensing applications: a review on graphene oxide, MoS2, WS2 and phosphorene, Sensors 18 (2018) 3638.

[20] Z. Yuan, Q. Zhao, Z. Duan, C. Xie, X. Duan, S. Li, Z. Ye, Y. Jiang, H. Tai, Ag2Te nanowires for humidity-resistant trace-level NO2 detection at room temperature, Sens. Actuat. B: Chem. 363 (2022) 131790.

[21] Y. Su, W. Li, X. Cheng, Y. Zhou, S. Yang, X. Zhang, C. Chen, T. Yang, H. Pan, G. Xie, High-performance piezoelectric composites via β phase programming, Nat. Commun. 13 (2022) 4867.

[22] C. Chen, M. Jiang, X. Luo, H. Tai, Y. Jiang, M. Yang, G. Xie, Y. Su, Ni-Co-P hollow nanobricks enabled humidity sensor for respiratory analysis and human-machine interfacing, Sens. Actuat. B: Chem. 370 (2022), 132441.

[23] Y. Zhang, Y. Jiang, Z. Duan, Y. Wu, Q. Zhao, B. Liu, Q. Huang, Z. Yuan, X. Li, H. Tai, Edge-enriched MoS2 nanosheets modified porous nanosheet-assembled hierarchical In2O3 microflowers for room temperature detection of NO2 with ultrahigh sensitivity and selectivity, J. Hazard. Mater. 434 (2022), 128836.

[24] Y. Zhang, Y. Jiang, Z. Yuan, B. Liu, Q. Zhao, Q. Huang, Z. Li, W. Zeng, Z. Duan, H. Tai, Synergistic Effect of Electron Scattering and Space Charge Transfer Enabled Unprecedented Room Temperature NO2 Sensing Response of SnO2, Small, 2303631.

[25] Y. Guo, B. Liu, Z. Duan, Z. Yuan, Y. Jiang, H. Tai, Batch fabrication of H2S sensors based on evaporated Pd/WO3 film with ppb-level detection limit, Mater. Chem. Phys.s 302 (2023), 127768.

[26] Y. Su, Y. Liu, W. Li, X. Xiao, C. Chen, H. Lu, Z. Yuan, H. Tai, Y. Jiang, J. Zou, Sensing–transducing coupled piezoelectric textiles for self-powered humidity detection and wearable biomonitoring, Mater. Horiz. 10 (2023) 842–851.

[27] R. Bogue, Graphene sensors: a review of recent developments, Sens. Rev. 34 (2014) 233–238.

[28] F. Schedin, A.K. Geim, S.V. Morozov, E.W. Hill, P. Blake, M.I. Katsnelson, K.S. Novoselov, Detection of individual gas molecules adsorbed on graphene, Nat. Mater. 6 (2007) 652–655.

[29] K. Vikrant, V. Kumar, K.-H. Kim, Graphene materials as a superior platform for advanced sensing strategies against gaseous ammonia, J. Mater. Chem. A 6 (2018) 22391–22410.

[30] F. Yavari, E. Castillo, H. Gullapalli, P.M. Ajayan, N. Koratkar, High sensitivity detection of NO2 and NH3 in air using chemical vapor deposition grown graphene, Appl. Phys. Lett. 100 (2012).

[31] D.J. Buckley, N.C. Black, E.G. Castanon, C. Melios, M. Hardman, O. Kazakova, Frontiers of graphene and 2D material-based gas sensors for environmental monitoring, 2D Materials 7 (2020) 032002.

[32] S. Aghaei, A. Aasi, S. Farhangdoust, B. Panchapakesan, Graphene-like BC6N nanosheets are potential candidates for detection of volatile organic compounds (VOCs) in human breath: A DFT study, Appl. Surf. Sci. 536 (2021), 147756.

[33] Z. Wang, C. Chen, H. Liu, D. Hrynshpan, T. Savitskaya, J. Chen, J. Chen, Enhanced denitrification performance of Alcaligenes sp. TB by Pd stimulating to produce membrane adaptation mechanism coupled with nanoscale zero-valent iron, Sci. Total Environ. 708 (2020), 135063.

[34] N. Goel, M. Kumar, Recent advances in ultrathin 2D hexagonal boron nitride based gas sensors, J. Mater. Chem. C 9 (2021) 1537–1549.

[35] F. Mofidi, A. Reisi-Vanani, Investigation of the electronic and structural properties of graphyne oxide toward CO, CO2 and NH3 adsorption: A DFT and MD study, Appl. Surf. Sci. 507 (2020), 145134.

[36] J. Huang, D. Jiang, J. Zhou, J. Ye, Y. Sun, X. Li, Y. Geng, J. Wang, Y. Du, Z. Qian, Visible light-activated room temperature NH3 sensor base on CuPc-loaded ZnO nanorods, Sens. Actuat. B: Chem. 327 (2021), 128911.

[37] D. Zhang, Z. Yang, P. Li, M. Pang, Q. Xue, Flexible self-powered high-performance ammonia sensor based on Au-decorated MoSe2 nanoflowers driven by single layer MoS2-flake piezoelectric nanogenerator, Nano Energy 65 (2019), 103974.

[38] E. Lee, D.-J. Kim, Recent exploration of two-dimensional MXenes for gas sensing: From a theoretical to an experimental view, J. Electrochem. Soc. 167 (2020), 037515.

[39] Y. Su, S. Chen, B. Liu, H. Lu, X. Luo, C. Chen, W. Li, Y. Long, H. Tai, G. Xie, Y. Jiang, Maxwell displacement current induced wireless self-powered gas sensor array, Mater. Today Phys. 30 (2023), 100951.

[40] Z. Liu, S. Liu, S. Er, Hydrogen storage properties of Li-decorated B₂S monolayers: a DFT study, Int. J. Hydrog. Energy 44 (2019) 16803–16810.

[41] G. Qin, Q. Cui, B. Yun, L. Sun, A. Du, Q. Sun, High capacity and reversible hydrogen storage on two dimensional C2N monolayer membrane, Int. J. Hydrog. Energy 43 (2018) 9895–9901.

[42] A. Hashmi, M.U. Farooq, I. Khan, J. Son, J. Hong, Ultra-high capacity hydrogen storage in a Li decorated two-dimensional C₂N layer, J. Mater. Chem. A 5 (2017) 2821–2828.

[43] S. Lu, J. Guo, S. Liu, B. Yang, M. Liu, L. Yin, W. Zheng, An improved algorithm of drift compensation for olfactory sensors, Appl. Sci. 12 (2022) 9529.

[44] E. Anikina, T. Hussain, V. Beskachko, R. Ahuja, Elucidating hydrogen storage properties of two-dimensional siligraphene (SiC 8) monolayers upon selected metal decoration, Sust. Energy Fuel 4 (2020) 5578–5587.

[45] S. Naqvi, T. Hussain, W. Luo, R. Ahuja, Metallized siligraphene nanosheets (SiC7) as high capacity hydrogen storage materials, Nano Res. 11 (2018) 3802–3813, in.

[46] X. Wang, H. Feng, T. Chen, S. Zhao, J. Zhang, X. Zhang, Gas sensor technologies and mathematical modelling for quality sensing in fruit and vegetable cold chains: a review, Trends Food Sci. Technol. 110 (2021) 483–492.

[47] R.Y. Sathe, T.D. Kumar, Reversible hydrogen adsorption in Li functionalized [1, 1] paracyclophane, Int. J. Hydrog. Energy 45 (2020) 12940–12948.

[48] A. Salehabadi, M.F. Umar, A. Ahmad, M.I. Ahmad, N. Ismail, M. Rafatullah, Carbon-based nanocomposites in solid-state hydrogen storage technology: an overview, Int. J. Hydrog. Energy Rsch 44 (2020) 11044–11058.

[49] S. Chandra, D. Roy Chowdhury, M. Addicoat, T. Heine, A. Paul, R. Banerjee, Molecular level control of the capacitance of two-dimensional covalent organic frameworks: role of hydrogen bonding in energy storage materials, Chem. Mater. 29 (2017) 2074–2080.

[50] L. Pasquini, Design of nanomaterials for hydrogen storage, Energies 13 (2020) 3503.

[51] J. Li, G. Xie, J. Jiang, Y. Liu, C. Chen, W. Li, J. Huang, X. Luo, M. Xu, Q. Zhang, M. Yang, Y. Su, Enhancing photodegradation of Methyl Orange by coupling piezo-phototronic effect and localized surface plasmon resonance, Nano Energy 108 (2023), 108234.

[52] L. Kong, G. Liu, Synchrotron-based infrared microspectroscopy under high pressure: an introduction, Matter Radiat. Extrem. 6 (2021) 12–20.

[53] H.G. Shiraz, O. Tavakoli, Investigation of graphene-based systems for hydrogen storage, Renew. Sust. Energ. Rev. 74 (2017) 104–109.

[54] V. Tozzini, V. Pellegrini, Prospects for hydrogen storage in graphene, PCCP 15 (2013) 80–89.

[55] V. Jain, B. Kandasubramanian, Functionalized graphene materials for hydrogen storage, JJ, Mater. Sci. 55 (2020) 1865–1903.

[56] O. Faye, J.A. Szpunar, B. Szpunar, A.C. Beye, Hydrogen adsorption and storage on Palladium–functionalized graphene with NH-dopant: A first principles calculation, Appl. Surf. Sci. 392 (2017) 362–374.

[57] A.N. Sosa, F. de Santiago, Á. Miranda, A. Trejo, F. Salazar, L.A. Pérez, M. Cruz-Irisson, Alkali and transition metal atom-functionalized germanene for hydrogen storage: a DFT investigation, Int. J. Hydrog. Energy 46 (2021) 20245–20256.

[58] H. Pan, G. Chen, Y. Chen, A. Di Carlo, M.A. Mayer, S. Shen, C. Chen, W. Li, S. Subramaniam, H. Huang, H. Tai, Y. Jiang, G. Xie, Y. Su, J. Chen, Biodegradable cotton fiber-based piezoresistive textiles for wearable biomonitoring, Biosens. Bioelectron. 222 (2023), 114999.

[59] Y. Wang, Q. Wu, J. Mao, S. Deng, R. Ma, J. Shi, J. Ge, X. Huang, L. Bi, J. Yin, Lithium and calcium decorated triphenylene-graphdiyne as potential high-capacity hydrogen storage medium: a first-principles prediction, Appl. Surf. Sci. 494 (2019) 763–770.

[60] Y. Guo, B. Xu, Y. Xia, J. Yin, Z. Liu, First-principles study of hydrogen storage on Ti-decorated B₂C sheet, J. Solid State Chem. 190 (2012) 126–129.

[61] U. Oleander, Lunar mineral extraction to correct for potential loss of Earth mass caused by fossil fuel consumption, Sci. Total Environ. 557 (2016).

[62] S. Kumar, R.Y. Sathe, T.D. Kumar, Sc and Ti-functionalized 4-tert-butylcalix [4] arene as reversible hydrogen storage material, Int. J. Hydrog. Energy 44 (2019) 12724–12732.

[63] R. Varunaa, P. Ravindran, Potential hydrogen storage materials from metal decorated 2D-C 2 N: an ab initio study, Phys. Chem. Chem. Phys. 21 (2019) 25311–25322.

[64] S. Jana, S. Thomas, C.H. Lee, B. Jun, S.U. Lee, B3S monolayer: Prediction of a high-performance anode material for lithium-ion batteries, J. Mater. Chem. A 7 (2019) 12706–12712.

[65] M.W. Schmidt, K.K. Baldridge, J.A. Boatz, S.T. Elbert, M.S. Gordon, J.H. Jensen, S. Koseki, N. Matsunaga, K.A. Nguyen, S. Su, General atomic and molecular electronic structure system, J. Comput. Chem. 14 (1993) 1347–1363.

[66] J. Beheshtian, A.A. Peyghan, Z. Bagheri, Detection of phosgene by Sc-doped BN nanotubes: a DFT study, Sens. Actuat. B: Chem. 171 (2012) 846–852.

[67] M.A. Abdulsattar, SiGe superlattice nanocrystal pure and doped with substitutional phosphorus single atom: density functional theory study, Superlatt. Microstruct. 50 (2011) 377–385.

[68] S. Tomić, B. Montanari, N. Harrison, The group III–V's semiconductor energy gaps predicted using the B3LYP hybrid functional, Phys. E: Low-Dimens. Syst. Nanostruct. 40 (2008) 2125–2127.

[69] M.M.T. O'Boyle, A L. and Langer, K MJ Comput. Chem. 29 (2008) 839.

[70] W.-Z. Yu, J.-A. Yan, S.-P. Gao, Band gap characters and ferromagnetic/antiferromagnetic coupling in group-IV monolayers tuned by chemical species and hydrogen adsorption configurations, Nanoscale Res. Lett. 10 (2015) 1–13.

[71] N. Al-Zaqri, T. Pooventhiran, F.A. Alharthi, U. Bhattacharyya, R. Thomas, Structural investigations, quantum mechanical studies on proton and metal affinity and biological activity predictions of selpercatinib, J. Mole. Liq. 325 (2021), 114765.

[72] S. Peng, K. Cho, P. Qi, H. Dai, Ab initio study of CNT NO₂ gas sensor, ChemPhys. Lett. 387 (2004) 271–276.

[73] O. Faye, U. Eduok, J.A. Szpunar, Boron-decorated graphitic carbon nitride (g-C3N4): an efficient sensor for H₂S, SO₂, and NH₃ capture, J. Phys. Chem. C 123 (2019) 29513–29523.

[74] B.J. Cid, J.E. Santana, L.G. Arellano, Á. Miranda, S.E. Pérez-Figueroa, M.I. Iturrios, L.A. Pérez, M. Cruz-Irisson, Metal-decorated siligene as work function type sensor for NH3 detection: a DFT approach, Appl. Surf. Sci. 610 (2023), 155541.

[75] A.N. Sosa, J.E. Santana, Á. Miranda, L.A. Pérez, A. Trejo, F. Salazar, M. Cruz-Irisson, NH3 capture and detection by metal-decorated germanene: a DFT study, J. Mater. Sci. 57 (2022) 8516–8529.

[76] V. Kumar, D.R. Roy, Single-layer stanane as potential gas sensor for NO₂, SO₂, CO₂ and NH₃ under DFT investigation, Phys. E: Low-Dimens. Syst. Nanostruct. 110 (2019) 100–106.

[77] L. Lin, Z. Feng, Z. Dong, C. Hu, L. Han, H. Tao, DFT study on the adsorption of CO, NO₂, SO₂ and NH₃ by Te vacancy and metal atom doped MoTe2 monolayers, Phys. E: Low-Dimens. Syst. Nanostruct. 145 (2023), 115489.